ELSEVIER

Journal of Nuclear Materials 301 (2002) 70–76

journal of nuclear materials

www.elsevier.com/locate/jnucmat

Liquid metal embrittlement of the martensitic steel 91: influence of the chemical composition of the liquid metal. Experiments and electronic structure calculations

A. Legris *, G. Nicaise, J.-B. Vogt, J. Foct

Laboratoire de Métallurgie Physique et Génie des Matériaux, UMR-CNRS 8517, Université des Sciences et Technologies de Lille, Bât C6, 59 655 Villeneuve D'Ascq cedex, France

Abstract

In previous works [Scripta Mater. 43 (2000) 997; J. Nucl. Mater. 296 (2001) 256], we showed that the martensitic steel 91 is prone to liquid metal embrittlement (LME) by liquid lead provided that some metallurgical conditions are fulfilled. In this work, we report results of LME of the steel 91 in contact with Pb–Bi and other low melting temperature metals such as Sn and Hg. Our experimental results can be interpreted within the framework of the surface energy reduction models for LME. To account for the experimental observations, we performed electronic structure calculations to assess the chemical interaction between low melting temperature metal atoms and iron surfaces. Our results allow to establish a simple criterion that can give trends on the embrittlement power of a liquid metal in contact with iron.

PACS: 62.20.Mk; 81.40.Np; 31.15.Ar

1. Introduction

The occurrence of liquid lead embrittlement of a martensitic steel Z10 CD Nb V 9-1 (AFNOR) steel (designated hereafter steel or grade 91) at temperatures close to the lead melting temperature has been recently reported [1,2]. To prompt the embrittlement, the adopted strategy consisted in increasing the material strength by using a well adapted thermal treatment and, combined to this, it was also necessary to machine a notch on the initially smooth cylindrical tensile specimens. Our experimental results clearly showed that the embrittlement by liquid lead disappears if the testing temperature is raised above 450 °C [2].

In this work we are dealing with results concerning the embrittlement of the grade 91 (submitted to a hardening heat treatment) by different liquid metals (the eutectic Pb–Bi, Sn and Hg). The corresponding binary phase diagrams Fe–liquid metal are different: the Fe–Pb–Bi and Fe–Hg systems on one side are nonmiscible while on the other side the Fe–Sn system has intermetallics like FeSn and $FeSn_2$. As will be shown, however, the mechanical response of the grade 91 in contact with the liquid metals cannot be deduced from these simple thermodynamic considerations since as far as the mechanical behaviour is concerned, the Fe–Pb–Bi system is closer to the Fe–Sn system than to the Fe–Hg one.

Given the experimental conditions adopted in this work, the observed embrittlement is very likely to be a direct consequence of the reduction of the steel surface energy due to the adsorption of liquid metal atoms as pointed out by Rehbinder and co-workers for instance [3]. The reduction of the surface energy by adsorption of liquid metal atoms can in principle be evaluated from atomic scale simulations relying on accurate models for the interaction potential energy between the different kinds of atoms. Here, we have performed electronic

* Corresponding author. Tel.: +33-3 20 33 63 83; fax: +33-3 20 43 40 40.

E-mail address: alexandre.legris@univ-lille1.fr (A. Legris).

0022-3115/02/$ - see front matter
PII: S0022-3115(01)00730-9

structure (ab initio) calculations to address the chemical interactions between the (1 0 0), (1 1 0) and (1 1 1) iron surfaces and Hg, Pb, Bi and Sn atoms. It will be shown that the calculation of the adsorption energies can give useful trends towards an LME prediction.

2. Experimental procedure

2.1. Base material

The base material supplied by Creusot Loire Industries is the Z10 CD Nb V 9-1 (AFNOR) steel designated steel or grade 91. Its chemical composition is given in Table 1. The as received material has a tempered martensitic microstructure resulting from the standard heat treatment consisting in heating 1 h at 1050 °C, air quenching, heating 1 h at 750 °C and then air cooling. Due to its low carbon content, its crystallographic structure is bcc, and the average grain size is about 20 μm [1,2].

2.2. Specimen preparation, tensile tests and fractography

Cylindrical tensile specimens with a 4 mm diameter and a gauge length of 20 mm were machined from the as received ingots. In order to increase as much as possible the steel hardness, a specific heat treatment was applied consisting in tempering the steel at 500 °C instead of 750 °C [1]. This did not change the crystallographic structure neither the grain size (which is only controlled by the austenitisation treatment). For all the specimens, a notch (depth = 500 μm, curvature radius = 200 μm) was mechanically machined.

The tensile tests were performed at constant stroke speed corresponding to a strain rate of 10^{-4} s^{-1} using a Schenck RMC 100 servo-electric test machine. For the high temperature tests, the temperature was reached using a standard three heating zones furnace. A 525M Philips scanning electron microscope in the secondary electron mode was used to perform the fractographic analysis.

2.3. Computational details

Our calculations were performed using the Vienna ab initio simulation package (VASP) [4]. This code implements the main concepts of the density functional theory (DFT) [5] combined with very efficient numerical algorithms for the self consistent resolution of the one-electron effective hamiltonian. The calculations are performed in a plane wave basis, using fully nonlocal Vanderbilt-type ultrasoft pseudopotentials to describe the electron–ion interaction [6]. Exchange and correlation are described by the Perdew and Zunger functional adding non-local corrections in the form of the generalised gradient approximation (GGA) of Perdew and Wang [7]. The pseudopotentials used were taken from the VASP library. In Table 2 we report their corresponding electronic configuration. A unique cut-off energy of 240 eV was used for all the systems. All the calculations were performed using spin polarisation. The supercell approach was used to simulate perfect crystals as well as slabs with free surfaces. Brillouin zone (BZ) sampling was performed using the Monkhorst and Pack and related schemes. A convergence within 2 meV per atom with respect to the discrete BZ sampling was achieved using a k-points density close to $4000V_{Fe}$, where V_{Fe} is the iron atomic volume. The (1 0 0) and (1 1 1) surfaces were modeled by six layers and the (1 1 0) surface was described using a four-layers slab. For the (1 0 0) surface a square surface cell was chosen and the total amount of Fe atoms in the simulation supercell was 24. For the (1 1 0) we used a rectangular surface cell and 16 Fe atoms in the supercell, and for the (1 1 1) surface there were 24 atoms in the supercell and the surface cell was rhombohedral. A top view of the three different supercells is displayed in Fig. 1.

Table 1
Chemical composition of the steel 91 used in this work

	Major elements								
	Cr	Mo	V	Mn	Si	Ni	C	Nb	Fe
wt%	8.80	1.00	0.25	0.38	0.41	0.17	0.11	0.07	Balance

Table 2
Electronic configuration of the pseudopotentials used in this work and Wigner–Seitz radius of each element

	Element				
	Fe	Pb	Bi	Hg	Sn
P.P. electronic shell	3d6 4s2	5d10 6s2 6p2	6s2 6p3	5d10 6s2	4d10 5s2 5p2
Wigner–Seitz radius (nm)	0.130	0.173	0.163	0.161	0.157

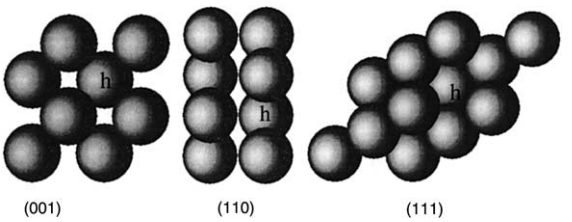

Fig. 1. Top view of the Fe supercells used to calculate the adsorption energies of different adatoms. Only the hollow sites (h) were tested as adsorption sites.

Whatever the adatom considered (Pb, Bi, Hg or Sn) only one adsorption site, the hollow one, noted 'h' in Fig. 1 was tested. Taking into account that all the adatoms considered are bigger than Fe (see their Wigner–Seitz radius in Table 2) it is very likely that the h sites are the preferential adsorption sites whatever the surface considered. In all the calculations the atoms near the surface were allowed to relax.

3. Results

3.1. Experimental results

All the tensile specimens were heat treated according to the treatment described in Section 2.2. All the tensile tests reported in this article were performed on notched specimens. Whatever the chemical environment, no particular care was taken to control the oxygen activity. Three test temperatures were adopted:

(i) 20 °C for the tests performed using liquid mercury. For safety reasons we did not perform tensile tests at higher temperatures using liquid Hg.
(ii) 260 °C for the tests performed using the eutectic Pb–Bi and liquid Sn.
(iii) 350 °C for the tests performed in contact with liquid lead.

Further experimental details concerning the experimental set-up and the tensile test realisation procedure can be found elsewhere [1,2].

Fig. 2 displays the force vs. elongation curves obtained at 20 °C in liquid mercury and in air. From these curves we can conclude that there is no noticeable difference in the mechanical behaviour of the material tested in the two different environments. While the fracture surfaces obtained at the same temperature in air using smooth specimens are characteristic of ductile failure, the fracture surfaces of the notched specimens were brittle in air and in liquid Hg. In Fig. 3 we show SEM micrographs of the fracture surfaces corresponding to the specimens of Fig. 2. The fracture surfaces correspond to transgranular brittle fracture and are similar to those previously reported [1,2] obtained in liquid lead at 350 °C.

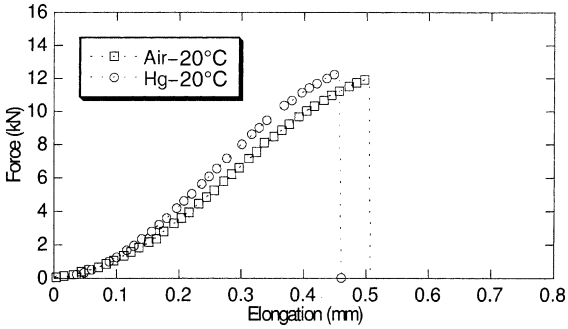

Fig. 2. Tensile test results of notched specimens obtained at 20 °C in air (open squares) and in liquid Hg (open circles).

In Fig. 4 we report the tensile tests results obtained at 260 °C in air, in the eutectic Pb–Bi and in liquid Sn. The results obtained at 350 °C in air and liquid Pb are also reported for comparison. It can be seen that both liquid Sn and the Pb–Bi eutectic have very similar detrimental

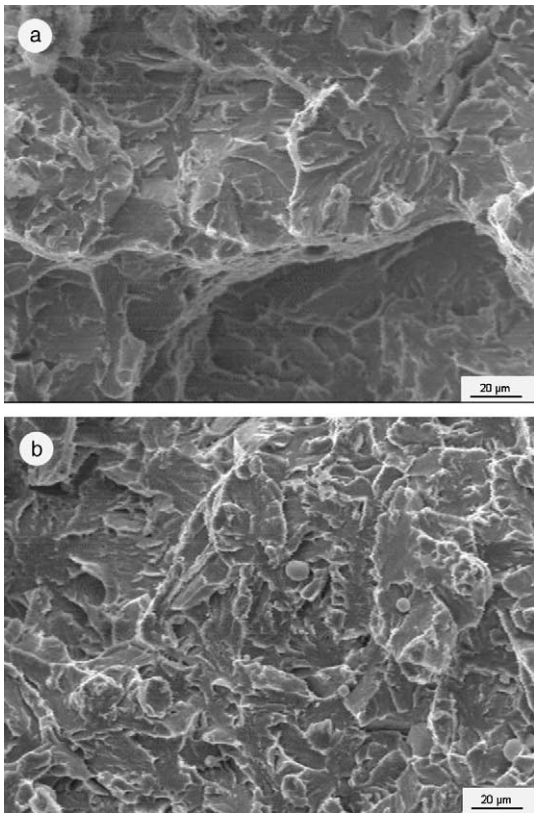

Fig. 3. SEM micrographs of the fracture surfaces obtained in air (a) and in liquid Hg (b) at 20 °C.

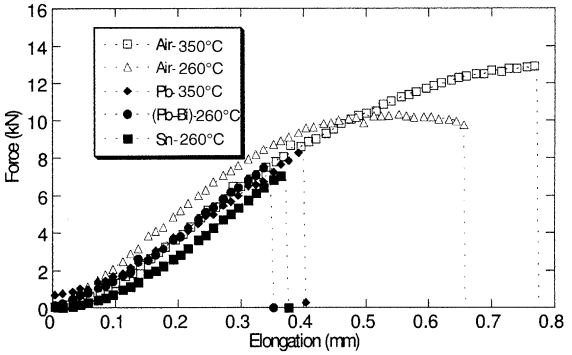

Fig. 4. Tensile test results of notched specimens obtained at 260 °C in liquid Sn (full squares), in the Pb–Bi eutectic (full circles), in air (open triangles) and at 350 °C in liquid lead (full diamonds) and in air (open squares).

effects on the mechanical properties of the material. The micrograph of Fig. 5(b) corresponding to the fracture surfaces of the specimens tested in the eutectic environment, are similar to those of Fig. 3 and indicate a brittle transgranular fracture. The fracture surfaces of the sample tested in air are, conversely, dimpled (Fig. 5(a)) indicating fully ductile fracture.

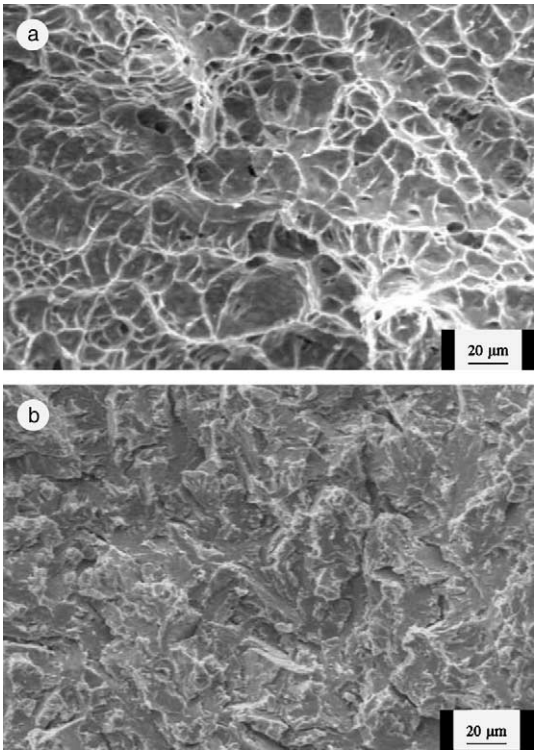

Fig. 5. SEM micrographs of the fracture surfaces obtained in air (a) and in the Pb–Bi eutectic (b) at 260 °C.

3.2. Adsorption energy calculations

In this section we describe the electronic structure calculations. We first report the results concerning the Fe surface energy calculations, γ_i, were i labels the surface index ((0 0 1), (0 1 1) or (1 1 1)). To obtain γ_i, we calculated the total energy of appropriate supercells containing two free surfaces of total area S each. At 0 K, the total energy E coincides with the reference free energy G^r that is given by

$$G^r = N_{Fe}\mu_{Fe} + 2S\gamma_i. \quad (1)$$

In expression (1), N_{Fe} is the number of Fe atoms in the simulation cell and μ_{Fe}, the Fe chemical potential, is the energy per Fe atom of pure bcc Fe at mechanical equilibrium, a quantity that can be easily calculated. The γ_i values obtained from this expression are shown in Table 3. They remarkably agree with an experimental average value $\gamma_{av} = 2.45$ J/m^2 [8] obtained from experiments with polycrystals. Furthermore, it can be noticed that the surface energy increase with decreasing surface density in agreement with an intuitive rule based on the number of broken bonds.

Starting from the pure Fe slabs with free surfaces, we deposited different adatoms on top of the hollow sites and let the ions relax. Fig. 6 displays a fully relaxed atomic configuration for Pb deposited on a (1 1 1) Fe surface. The calculation supercell was periodically repeated in the surface plane for clarity.

The free energy G, of an atomic configuration like that of Fig. 6 can be decomposed as follows:

$$G = N_{Fe}\mu_{Fe} + N_{ad}\mu_{ad} + S\gamma_i^{ad} + S\gamma_i, \quad (2)$$

where N_{ad} is the number of adsorbed atoms of type ad, μ_{ad} their chemical potential and γ_i^{ad} the surface energy modified by the adsorption of atom ad. Whatever the type of the adsorbed atom, μ_{ad} was taken at the energy per atom of the most stable condensed phase of the element ad at 0 K. This value is close to the value of the chemical potential of the liquid metal if the temperature dependence of the free energy and the latent heat of fusion are, to a good approximation, neglected. We then defined the adsorption energy E^{ad} for each species as

Table 3
Calculated Fe surface energy values for various surface orientations. The experimental value, obtained from polycrystalline Fe is an average value

	Surface index			
	0 0 1	0 1 1	1 1 1	Average (exp. [9])
Surface energy (J/m^2)	2.315	2.279	2.576	2.45

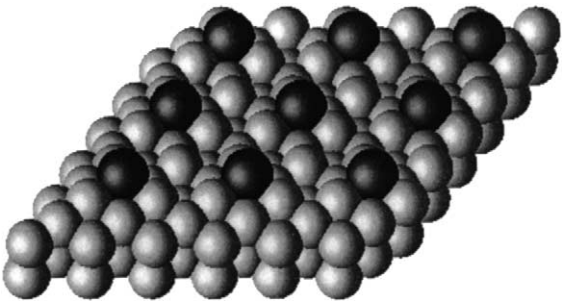

Fig. 6. Relaxed atomic structure of a Pb atom adsorbed at a Fe(1 1 1) surface. The supercell was periodically reproduced in the surface plane for clarity reasons.

$$E^{\mathrm{ad}} = -(G - G^{\mathrm{r}} - N_{\mathrm{ad}}\mu_{\mathrm{ad}}). \tag{3}$$

The calculated values are reported in Table 4.

An alternative way to present the same results is to calculate $\gamma_{\mathrm{i}}^{\mathrm{ad}} = \gamma_{\mathrm{i}} - E^{\mathrm{ad}}/S$ for the coverage fraction $\theta = 0.25$ used for all the surfaces. The results are given in Table 5. The values corresponding to the Pb–Bi eutectic are obtained from those of Pb and Bi weighted by the volume fraction of each element.

The results of Tables 4 and 5 deserve at least two important comments:

(i) if the reduction of surface energy for dilute adsorption is taken as an embrittlement indicator, then the embrittlement power of the different elements should be Hg $\ll$ Pb $<$ Sn $\sim$ Pb–Bi $<$ Bi,

(ii) whatever the element, for $\theta = 0.25$, the reduction of surface energy is higher for the (0 1 1) surfaces (note a reduction of 39% for Bi), the lower reduction being obtained for the (1 1 1) surfaces.

Table 4
Calculated values of the adsorption energies at different Fe surfaces for the adatoms investigated in this work

	Adsorbed element			
	Pb	Bi	Hg	Sn
0 0 1 E^{ad} (eV)	0.720	1.309	0.402	0.941
0 1 1 E^{ad} (eV)	0.874	1.268	0.599	0.900
1 1 1 E^{ad} (eV)	1.166	1.618	0.729	1.504

Table 5
Calculated values of the surfaces energies with adsorbed chemical species

	Adsorbed element				
	Pb	Bi	Pb–Bi	Hg	Sn
$\gamma_{001}^{\mathrm{ad}}$ (J/m^2)	1.957	1.665	1.796	2.115	1.848
$-\Delta\gamma/\gamma$ (%)	15	28	22	9	20
$\gamma_{011}^{\mathrm{ad}}$ (J/m^2)	1.665	1.388	1.512	1.858	1.647
$-\Delta\gamma/\gamma$ (%)	27	39	35	18	28
$\gamma_{111}^{\mathrm{ad}}$ (J/m^2)	2.241	2.112	2.170	2.367	2.144
$-\Delta\gamma/\gamma$ (%)	13	18	16	8	17

4. Discussion

From the results of Figs. 2 and 3, it can be seen that the notched and heat treated specimens tested in air and in liquid Hg at 20 °C undergo brittle fracture. The small differences in the mechanical response of both specimens can be attributed to differences in the notches, that we recall, are mechanically machined. Therefore, from these results, we can conclude that liquid mercury does not produce a supplementary embrittlement of the 91 steel tested in severe experimental conditions. Conversely, the samples tested at 260 °C in liquid Sn and in contact with the Pb–Bi eutectic are prone to LME when compared with the samples tested in air at the same experimental conditions (Figs. 4 and 5). As previously mentioned for the specimens tested at 20 °C, the differences of the mechanical response between the samples tested in liquid Sn and in the Pb–Bi can be due to differences in their notches. The fracture surfaces produced in contact with the eutectic are similar to those of Fig. 2 and those previously reported [1,2] concerning brittle fracture in liquid Pb. The fracture surfaces of the sample tested in liquid Sn remained covered by tin despite the usual electrochemical dissolution procedure used to clean them off of other deposited liquid metals (Pb, Pb–Bi and Hg for instance) and are not presented here. Therefore, our experimental results indicate an embrittlement power of liquid Sn similar to that of the Pb–Bi eutectic, and probably of the same order of magnitude of that of liquid lead. Concerning liquid Hg, we were not able to prompt any apparent embrittlement of the steel.

Concerning the reasons of the embrittlement, we believe that the reduction of the surface energies of the solid metal by the liquid one is the crucial phenomenon as pointed out by several authors [3,9–11] and indicated by our experimental results [1,2]. In the case of truly brittle materials like some glasses or ceramics, the Griffith criterion applies to calculate the crack propagation applied stress, σ_{p}, which, for a semi-elliptical crack of length c is given by

$$\sigma_{\mathrm{p}} = \sqrt{\frac{2E\gamma_{\mathrm{s}}}{\pi c}}, \tag{4}$$

where E is the young modulus and γ_{s}, the surface energy. Orowan proposed to extend the Griffith results to ductile materials with a small plastic zone ahead of the crack tip by replacing the expression (4) by

$$\sigma_{\mathrm{p}} = \sqrt{\frac{2E\gamma_{\mathrm{p}}}{\pi c}}, \tag{5}$$

where γ_p is an effective surface energy term that takes into account the energy dissipated by the dislocations motion during the crack advance. In metals, γ_p is at least three orders of magnitude greater than γ_s but it is important to keep in mind that γ_p is a monotonous increasing function of γ_s, even if the actual relationship between γ_s and γ_p is not known with precision [12]. Therefore a reduction of γ_s can induce an important decrease of the σ_p value given by the expression (5). Consequently, the evaluation of the surface energy reduction induced by the adsorption of liquid metals, leads to an indirect (because the actual relationship between γ_p and γ_s is not known) indicator of the embrittlement power of a given liquid metal.

In principle, the interface energy between the liquid and the solid metal can be calculated from atomic scale simulations if the interaction energy between the different kinds of atoms is known. To describe the potential energy, one can adopt empirical potentials that allow to handle thousands of atoms at the cost of an unknown transferability. This means that these energy models will reproduce accurately the energy of those atomic configurations used to fit the adjustable parameters of the potential (in general equilibrium configurations), but little can be inferred when the configurations of interest are apart of these, in particular when one deals with alloys. An alternative approach is to use accurate DFT based ab initio calculations that are transferable. In this case, the size of tractable systems by standard computers, is reduced to no more than one hundred atoms due the computational cost of this type of calculations. In this work we have chosen the second approach, the steel 91 being modelled by pure iron. Furthermore, given the important misfit between Fe and the others atoms of interest (see the Wigner–Seitz radius in Table 2) it is necessary to use supercells with large dimensions in the interface plane in order to model a solid–liquid interface, which rules out the use of ab initio calculations. Since we are interested here to know trends about the embrittlement power of a given liquid metal, and given the fact that from the Orowan's criterion the interface energy can only give qualitative information, we adopted here a different strategy that allows the chemical interaction between lead surfaces and liquid metals atoms to be characterised. To this end we calculated the adsorption energies reported in Table 4 for diluted surface coverage fractions, which are quantities much easier to compute than the true interface energies γ. This procedure, that can be considered as a first order approximation towards the calculation of γ, is commonly used by meaningful physical models in surface science (the Langmuir model) and materials science (the Mc Lean segregation model see Ref. [13] for instance) to address the surface adsorption and the grains boundaries segregation.

The fact that the adsorption energies calculated using formula (3) and reported Table 4 are positive means that in presence of an iron surface, it is energetically favourable to extract a liquid metal atom from a reservoir containing the pure liquid at its equilibrium chemical potential and to place it at the iron surface, and this whatever the liquid metals atoms considered. Such a conclusion cannot be made from phase equilibrium diagrams that only consider bulk phases, and is in particular independent of the existence of intermetallic phases (compare Sn and the other metals atoms). Expressing the adsorption energies as surfaces energies γ_i^{ad} (results of Table 5) allows a embrittlement criterion to be established as indicated in the previous section. The results reported in Table 5, obtained for low coverage fractions, are to be considered as upper bounds for the γ_i^{ad} values, and work is in progress to take into account lateral interactions between adsorbed atoms (beyond the Langmuir approximation). At this stage however, it is remarkable how a such simple model can give the correct experimentally observed trends.

5. Conclusions

In this article we present experimental and atomic simulation results of the influence of the chemical composition of the liquid bath on the embrittlement of the grade 91 steel. Working with heat treated samples, allowed us to show the existence of an embrittlement in different liquid metals environments and to establish an experimental scale of embrittlement. Ab initio atomic scale simulations combined to a very simple thermodynamic model allowed us to build a theoretical embrittlement scale based on the reduction of the surface energy by liquid metals adsorption, that corresponds to the experimental one. This work, presenting results concerning materials of technological interest, contributes to the fundamental understanding of the elementary mechanisms involved in LME.

Acknowledgements

We are indebted to P. Bocquet from Creusot–Loire Industries for providing the steel 91. This work has been supported by the French CNRS GdR GEDEON and by the EMA Department of EDF that we would like to thank. It has partially benefited from the computational facilities of the French organizations IDRIS and CINES as well as those of the CRI-USTL supported by the Fonds Européens de Développement Régional. We are also indebted to our colleague R. Besson for very fruitful scientific discussions.

References

[1] A. Legris, G. Nicaise, J.-B. Vogt, J. Foct, D. Gorse, D. Vançon, Scripta Mater. 43 (2000) 997.
[2] G. Nicaise, A. Legris, J.-B. Vogt, J. Foct, J. Nucl. Mater. 296 (2001) 256.
[3] E.D. Shchukin, Coll. Surf. A 149 (1999) 529.
[4] G. Kresse, J. Hafner, Phys. Rev. B 47 (1993) 558; G. Kresse, J. Hafner, Phys. Rev. B 49 (1994) 14251; G. Kresse, J. Furthmüller, Phys. Rev. B 54 (1996) 11169; G. Kresse, J. Furthmüller, Comput. Mater. Sci. 6 (1996) 15.
[5] P. Hohenberg, W. Kohn, Phys. Rev. 136 (1964) 864; W. Kohn, L. Sham, Phys. Rev. 140 (1965) 1133.
[6] D. Vanderbilt, Phys. Rev. B 41 (1990) 7892; G. Kresse, J. Hafner, J. Phys.: Condens. Mater. 6 (1996) 8245.
[7] J.P. Perdew, Y. Wang, Phys. Rev. B 45 (1991) 13244.
[8] H. Wawra, Z. Metallkd. 66 (1975) 395, 492.
[9] M.H. Kamdar, Prog. Mater. Sci. 15 (1973) 289.
[10] C.F. Old, J. Nucl. Mater. 92 (1980) 2.
[11] B. Joseph, M. Picat, F. Barbier, Eur. Phys. J. AP 5 (1999) 19.
[12] B. Lawn, Fracture of brittle solids, in: E.A. Davis, I.M. Ward (Eds.), Cambridge Solid State Science Series, 2nd Ed., Cambridge University, Cambridge, 1993.
[13] M. Guttmann, Metall. Trans. A 8 (1977) 1383.